Journal of Sound and Vibration (2000) **236**(3), 505–527
doi:10.1006/jsvi.2000.2991, available online at http://www.idealibrary.com on IDEAL®

NUMERICAL CONTROL OF IMPACT DYNAMICS OF INVERTED PENDULUM THROUGH OPTIMAL FEEDBACK STRATEGIES

S. LENCI

Istituto di Scienza e Tecnica delle Costruzioni, Università di Ancona, via Brecce Bianche, Monte D'Ago, 60131 *Ancona, Italy*

AND

G. REGA

Dipartimento di Ingegneria Strutturale e Geotecnica, Università di Roma "La Sapienza", via A. Gramsci 53, 00197 *Roma, Italy*

(*Received* 18 *January* 1999, *and in final form* 28 *February* 2000)

The problem of controlling the impact dynamics of an inverted pendulum is addressed. Starting from the optimal excitation for avoiding chaos obtained in previous works, interest is in increasing its practical performance and its application range. Two different implementations of the control procedure are developed in order to fulfil specific technical requirements of the system dynamics. They involve alternate use of one-side optimal and harmonic excitations, aimed at increasing the time spent by the hitting mass in the controlled potential well; or of right and left optimal excitations, aimed at reducing the scattered nature of the response as synthesized by the number of jumps between the two wells. The two implementations realize feedback control strategies which, however, require only minor information on the dynamics. Numerical simulations are performed to show their effectiveness, to compare them on a local and global basis, and to describe qualitative and quantitative aspects of the two requirements achieved with the proposed strategies.

1. BACKGROUND AND MOTIVATION

The possibility of controlling non-linear dynamics and chaos by avoiding homoclinic intersections occurring in the dynamics of mechanical systems has recently been investigated by the authors, both theoretically [1] and by means of numerical simulations [2]. The central key, inspired by a work of Shaw [3], consists of choosing the best periodic excitation which permits the critical threshold for the homoclinic bifurcation to increase. For a fixed period, this has been achieved by varying the *shape*, i.e., the Fourier coefficients, of the external input, and *optimal* excitations have been obtained [1].

The method proposed by the authors adds to the numerous existing methods for controlling non-linear dynamics and chaos, such as, for example, the classical methods of control [4, 5], the "control by the system design" [6, 7], the so-called OGY's method [8], the "parametric variation methods" [9], the "control through operating conditions" [6, 7] and all the techniques based on modifications of a basic harmonic excitation [3, 10]. Also mentioned are the open-loop strategies, engineering feedback controls, optimal controls,

0022-460X/00/380505 + 23 $35.00/0

adaptive controls, intelligent controls and so on, which are summarized in Chen and Dong's book [11] and also by Brogliato [12].

By applying the proposed method to mechanical systems with two-well potentials one basic difference arises. In fact, these systems have two homoclinic loops, and a choice must be made as to whether one wants to avoid *only one* of the two homoclinic bifurcations or *simultaneously* both bifurcations. These cases are called *one-side* and *global* control, respectively, and they have been extensively investigated by the authors [1, 2, 13, 14]. In these works, it has been shown how they are effective in terms of controlling the non-linear dynamics of the system and of regularizing its chaotic dynamics.

In order to increase the practical performances of the method, two implementations of the optimal procedure have been proposed and preliminarily tested [15]. They involve an alternate use of one-side optimal and harmonic excitations. More precisely, the first, called "optimal–harmonic", consists of applying the one-side optimal excitation when the system oscillates in the controlled potential well (i.e., the potential well where the homoclinic bifurcation has been avoided) and applying the harmonic excitation when the system state is elsewhere. The latter, on the other hand, called "optimal–optimal", entails a shrewd alternation of right and left one-side optimal excitations. From the control theory point of view, the proposed procedures require knowledge of the state of the system, and therefore they can be classified as feedback control strategies, contrary to the open-loop controls employed in the other authors' works. However, as will be seen in due course, it is not necessary to know the exact position and velocity of the system, but only minor information such as the occupied potential well, and therefore the implementations can probably be reproduced easily in practice.

The aim of this paper is to perform an extended numerical study of these procedures and to show their effectiveness in terms of steadily realizing some practical requirements of the system dynamics. In fact, apart form the necessity of improving the *general* performances of the method, the feedback strategies are introduced to improve at least two *specific* properties. The first is the length of stay in the controlled potential well. In some practical situations, in fact, it may be desirable to keep the system in one of the two potential wells as long as possible, and this can be achieved by the optimal–harmonic implementation, as it will be illustrated in section 4.

The second property, on the other hand, is the number of jumps between the two potential wells. In several cases, and in particular in the case of the impacting pendulum considered in section 2, the number of jumps is strictly related to the lifetime of the system, and the necessity to reduce it arises from the attempt to increase the lifetime. This issue will be dealt with in section 5 by the introduction and analysis of the coefficient of reduction of jumps between the two potential wells, a number which synthesizes the performance of the implementation.

Both these properties are concerned, from different points of view, with the comparison between the scattered and bounded nature of the motion. More precisely, their improvement is strictly related to the reduction of the scattered character of the solutions. Indeed, by construction, it makes sense to use the feedback strategies only when scattered dynamics appear in the system optimal response. As shown in reference [2], this occurs for very high values of the excitation amplitude (denoted by γ_1), quite close to the homoclinic bifurcation values. Thus, the natural parameter regions for using the implementations are those corresponding to high excitation amplitudes, on which attention is mainly focused.

In this paper, the proposed method is applied in order to improve the performances of the inverted pendulum subjected to periodic excitation. In addition to the theoretical interest, the pendulum is herein assumed as a paradigm for a large class of more realistic systems whose study permits the detection of some important dynamic phenomena and the

evaluation of the effectiveness of control schemes. Indeed, it is worth noting that the strategies employed do not depend on this specific system. The ideas behind the method apply to a large class of systems of practical interest, certainly to all two-well oscillators. The optimal open-loop excitations which alternate in the feedback implementations actually depend on the system, but they can be (exactly or approximately) computed for many mechanical systems.

2. THE MECHANICAL MODEL AND THE CONTROL METHOD

The equations of motion of the inverted pendulum with rigid unilateral constraints subjected to base periodic excitation (see Figure 1) are

$$\ddot{x} + 2\delta\dot{x} - x = f(t), \quad |x| < 1,$$
$$\dot{x}(t^+) = -r\dot{x}(t^-), \quad |x| = 1, \tag{1}$$

where $x = \vartheta/\vartheta_{max}$, ϑ is the deflection angle measured from the vertical, $\delta \in [0, 1[$ is the damping coefficient of free motion, $r \in]0, 1]$ is the coefficient of restitution for the *instantaneous* impacts and $f(t) = \sum_{j=1}^{\infty} \gamma_j \sin(j\omega t + \psi_j)$ is the T-periodic excitation force ($T = 2\pi/\omega$). In equation (1), Newton's law of impact is utilized. This model represents an approximation in describing the complicated phenomenon of impact, although this permits suitable computations. If the impacting bodies are sufficiently stiff and the impact time is very short, a situation that frequently occurs in practical applications, model (1) gives acceptable results, although more complex models are required if impacts cannot be considered as instantaneous.

Here the general analysis, which is detailed in reference [1] is briefly summarized.

In the phase space $(x, \dot{x})$, two homoclinic symmetric loops exist for the trival saddle $x \equiv 0$ of the unperturbed ($\delta = 0, r = 1, f(t) = 0$) system. When the excitation is added, on the Poincarè sections $\Sigma_{r,l} = \{(x, y, t) \in [-1, 1] \times \mathbb{R} \times S | x = \pm 1, y > 0\}$, the right and left distance between the stable and unstable manifolds is measured by

$$d_{r,l}(\tau) = \pm C_0/2 + \gamma_1 C_1 h(\tau),$$
$$h(\tau) = \sin(\tau + \Phi_1) + \sum_{j=2}^{\infty} \frac{\gamma_j C_j}{\gamma_1 C_1} \sin(j\tau + \Phi_j),$$
$$\Phi_j = \psi_j + \phi_j + v_j, \quad j = 1, 2, 3, \ldots. \tag{2}$$

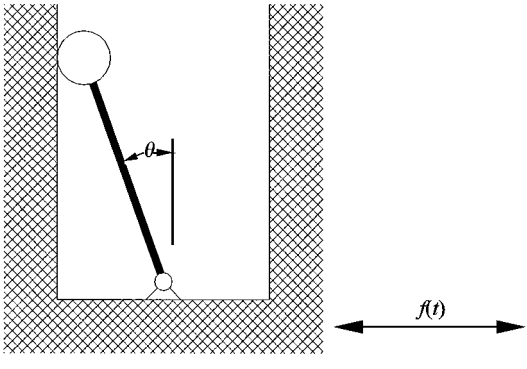

Figure 1. The inverted pendulum with rigid unilateral constraints.

Here $\tau = \omega t \in [0, 2\pi]$ and the parameters C_j, ϕ_j and v_j depend on j, ω, δ, r (see reference [1]). Let $M^r = \max_{\tau\in[0,2\pi]}\{h(\tau)\}$, $M^l = -\min_{\tau\in[0,2\pi]}\{h(\tau)\}$ and $\mu = \max\{M^r, M^l\}$. From equation (2), the necessary conditions for avoiding *independently* right or left transverse homoclinic intersections are

$$\gamma_1 < \left(-\frac{C_0}{2C_1}\right)\frac{1}{M^{r,l}} \stackrel{\text{def}}{=} \gamma^{r,l}_{1,cr}, \tag{3}$$

while a necessary condition for $d_{r,l}(\tau) \neq 0$ *simultaneously* is

$$\gamma_1 < \left(-\frac{C_0}{2C_1}\right)\frac{1}{\mu} \stackrel{\text{def}}{=} \gamma^{g}_{1,cr}. \tag{4}$$

In equation (3) only the right intersection will be considered, the analysis of the left case being the same. The functions $\gamma^r_{1,cr}$ and $\gamma^g_{1,cr}$ depend on ω (pulsation of the excitation) as well as on the other system parameters. In the space (ω, γ_1), they separate the non-chaotic region (below the critical curve) from the possibly chaotic region (above the curve). In the case of harmonic excitation, $h(\tau) = \sin(\tau + \Phi_1)$, $M^{r,l} = \mu = 1$ and $\gamma^h_{1,cr}$ is defined as the corresponding critical curve (see Figure 2, where each curve corresponds to a given excitation).

The aim of the control method is to maximize (by varying all the Fourier coefficients $\gamma_j, j = 2, 3, \dots$) the parameter $G = \gamma_{1,cr}/\gamma^h_{1,cr}$, which is called the *gain*. It represents the ratio between the critical amplitude of the actual excitation and the critical amplitude of the harmonic excitation, which is considered as a reference to measure the relative improvement of the proposed solution. In order to avoid only one homoclinic intersection (equation (3)), $G = \gamma^r_{1,cr}/\gamma^h_{1,cr} = 1/M^r$ (or $G = \gamma^l_{1,cr}/\gamma^h_{1,cr} = 1/M^l$) must be maximised, and the right (left) optimal problem is given. In order to avoid simultaneously both the homoclinic intersections (equation (4)), on the other hand, the higher value of $G = \gamma^g_{1,cr}/\gamma^h_{1,cr} = 1/\mu$ is sought and the global optimal problem is found.

The solution of the right optimal problem is the excitation

$$f^r(t) = f^*(t) + \frac{\gamma_1 C_1 r\pi}{2(1+r)\sin(\pi/(1-c))}\left[-\delta\left(t - \frac{\pi}{2\omega}\frac{1-3c}{1-c}\right) + \delta\left(t - \frac{\pi}{2\omega}\frac{5-3c}{1-c}\right)\right], \tag{5}$$

where $f^*(t)$ is a bounded function, $\delta(t)$ is the Dirac delta function, $c \leqslant -1$ is a parameter introduced for mathematical reasons. The solution of the left optimal problem is given by $f^l(t) = f^r(T - t)$, $t \in [0, T]$, while the solution of the global optimal problem is just the $f^r(t) = f^l(t)$ with $c = -1$.

The method for controlling chaos based on the substitution of the harmonic excitation with the function $f(t)$ given in equation (5) is called *one-side control*. The words "right" ("left") and "open-loop" (which underline that the right (left) homoclinic intersection is avoided and that the method is conceptually different form the feedback implementations that will be discussed in the following) are usually omitted. The method based on the use of the solution of the global optimal problem is called *global* (*open-loop*) *control*.

From a physical point of view, equation (5) means that, apart from $f^*(t)$, the optimal excitation consists of a couple of equal and opposite impulses with amplitude proportional to c. The best gain, which corresponds to equation (5), is

$$G = 2\frac{1-c}{\pi}\sin\left(\frac{\pi}{1-c}\right), \tag{6}$$

i.e., a theoretical gain up to 2 is feasible. For the global control, $G = 4/\pi \cong 1{\cdot}273$.

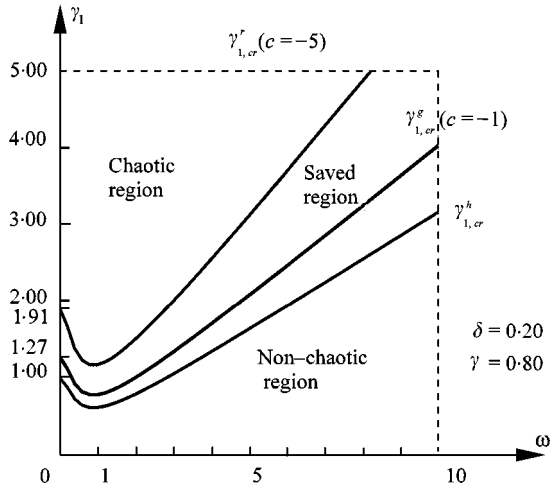

Figure 2. The critical curves $\gamma^r_{1,cr}$, $\gamma^g_{1,cr}$ and $\gamma^h_{1,cr}$.

3. FEEDBACK NUMERICAL IMPLEMENTATIONS OF THE CONTROL PROCEDURE

In the amplitude excitation range where they are theoretically expected to work, i.e., for $\gamma_1 < \gamma_{1,cr}$, the global and the one-side controls are most effective in controlling the non-linear dynamics of the system and in reducing its overall chaoticity. In particular, the authors [2] have shown numerically that the regularization of the dynamics reveals itself basically by the appearance of windows of periodic attractors within the underlying path of chaotic attractors. With global control these windows are already very large, and with the one-side control they become predominant. Furthermore, the optimal controls greatly influence the global system dynamics as well, by modifying the attractor-basin-manifold structure and the bifurcation paths. The existence of a non-classical local bifurcation which is related to the synchronization of impulses and impacts is noted [16].

Besides regularization, there are other performances of the optimal controls which have more technical interest. The more important one is likely to be the considerable increase, related to the gain, of the excitation amplitude value corresponding to the onset of scattered dynamics with respect to the reference excitation [2]. Also the well-defined mechanism of control, consisting of driving the dynamics into the controlled potential well where it is successively regularized, deserves some attentions. Both these aspects induce confinement of the dynamics into one of the two potential wells, and in some applications this circumstance may be more important than its actual regularization. Indeed, there are cases where even chaotic confined attractors may be preferable with respect to scattered periodic attractors.

In this paper, these technical results also for large values of the excitation amplitude are sought especially where the optimal excitations exhaust their natural (theoretical and practical) resources. Obviously, it is unlikely that full confinement of the dynamics for every large value of γ_1 will be achieved, and some weaker, though still useful from a practical point of view, performance must be accepted.

Attention is focused on two important by-products of the confinement, namely, the possibility of having mass in the desired potential well and the possibility of reducing the number of jumps between the wells. For large values of γ_1 these requirements cannot be fulfilled by the optimal excitations, so in the following sections two implementations only aimed at obtaining satisfactory results at the upper boundary (and even above the boundary) of the theoretically saved regions will be developed.

3.1. THE "OPTIMAL–HARMONIC" FEEDBACK IMPLEMENTATION

Initially, consider the case in which the aim is to have, as far as possible, the mass on the right part: here the one-side optimal excitation can be applied. If, incidentally, the mass escapes, it should come back to the right as soon as possible. This result could be obtained if, on the left, the dynamics are as chaotic as possible, therefore having an intrinsic propensity to change the potential well. Since the best chaoticity is furnished by the harmonic excitation, this excitation is switched to. After the mass has come to the right, the one-side control can be applied again, and so on indefinitely. It is natural to name this implementation "optimal–harmonic".

The idea which is the central key of this kind of implementation, is inspired by the OGY method [8]. As in this procedure, in fact use is made of the chaoticity of the dynamics to lead the solution into the part of the phase space where the control works adequately. Here the target zone is much larger (one-half of the phase space versus a neighbourhood of a given saddle), so that the solution should (and actually will) need a smaller amount of time to approach the target.

It is worth remarking that the proposed implementation depends on the state of the system, and therefore it seems to belong to the general class of the feedback controls. In spite of this, exact knowledge of the state of the mass is not required, but only minor information concerning the occupied potential well.

In the following numerical simulations, the excitation will be changed when the mass touches a rigid constraint. Right optimal excitation will be applied as far as the solution belongs to the right part of the phase space, while the optimal will be substituted by the harmonic excitation when the mass impacts the left constraint. On the right impacts, on the other hand, the optimal replaces the harmonic excitation. This method requires knowledge of the state of the system only at the impacts, and so it is relatively easy to reproduce in practice.

3.2. THE "OPTIMAL–OPTIMAL" FEEDBACK IMPLEMENTATION

If the number of jumps of the hitting mass from one to the other potential well is to be globally reduced, the best implementation of the procedure is likely to consist in using right optimal excitation if the solution belongs to the right potential well and left optimal excitation in the other case. Indeed, in this case it should be possible to maintain the mass in one of the two wells as far as possible and when it accidentally escapes, the other excitation should do the same work in the other part of the phase space.

This case will be labelled as "optimal–optimal" feedback implementation. As in the previous case (section 3.1), in the numerical simulations the excitation will be changed when the mass impacts on the rigid constraints, i.e., right optimal excitation will be set at right impacts and left optimal excitation will be set at left impacts.

From a practical point of view, reducing the jumping of the mass can be useful in different situations. For example, it diminishes the number and the intensity of the impacts, so prolonging the life of the structure. Furthermore, it is expected to be associated, at least in each potential well, with fairly regular solutions.

4. THE TIME SPENT IN THE CONTROLLED POTENTIAL WELL

By construction, the optimal–harmonic implementation should be able to increase the time spent by the mass in the controlled (right) potential well. In this section, some

numerical simulations are made to check how satisfactorily this result can be obtained. A classical fourth order Runge–Kutta–Fehlberg's method has been employed with $dt = T/1000$ for $|x| \leqslant 0{\cdot}97$ and $dt = T/30\,000$ for $0{\cdot}97 < |x| < 1$. This choice is justified by the need to better simulate the rebounding process. The following parameters are selected: $\delta = 0{\cdot}20$, $r = 0{\cdot}80$ and, in the case of fixed initial conditions (i.c.) $x_i = 0{\cdot}80$ and $\dot{x}_i = 0{\cdot}00$ one assumed. Furthermore, $c = -5$ is assumed and a two-impulse approximation of the optimal excitation is used, i.e., the $f^*(t)$ in equation (5) is neglected. This choice is motivated by the fact that this approximation if very close to the best $f(t)$ and it gives good results in the case of open-loop excitations [1, 2]. However, other approximations, more easily implemented in the system, are also possible. They seem to not modify greatly the *technical* performances obtained with the proposed method, as shown in reference [15], where the same feedback implementations are investigated but the optimal excitation is approximated by its Fourier series truncated to the first five terms. Another possibility is to consider *bounded* optimal excitations [17], instead of unbounded optimal excitations.

4.1. SYSTEM LOCAL ANALYSIS

For fixed i.c., Figure 3 shows (corresponding to $\omega = 5$ and $\gamma_1 = 3{\cdot}05$) the percentage of the total time spent in the right well versus the total time. In order to analyze the steady dynamics, the total time is extended up to $t = 20\,000T$. For $\omega = 5$ the *theoretical* critical threshold for chaos is $\gamma^r_{1,cr} \cong 3{\cdot}116$, while the *actual* one (due to the two impulses approximation) is reduced to $\gamma^r_{1,cr} \cong 2{\cdot}982$ [2, Part II]. Thus, the example considered is beyond the upper boundary of the actual saved region.

With the optimal–harmonic implementation the mass asymptotically spends 85.2% of the total time in the right potential well, while in the case of optimal–optimal excitation this value is 49·3%. For the sake of completeness and comparison, the cases of harmonic, global, right optimal and left optimal excitations are also reported, which give 48·7, 49·5, 22·5 and 77·5% of the time in the right well, respectively. These numbers, and also Figure 3, clearly show the effectiveness of the optimal–harmonic implementation for large values of γ_1. In particular, the time spent in the desired potential well can be increased with respect to the

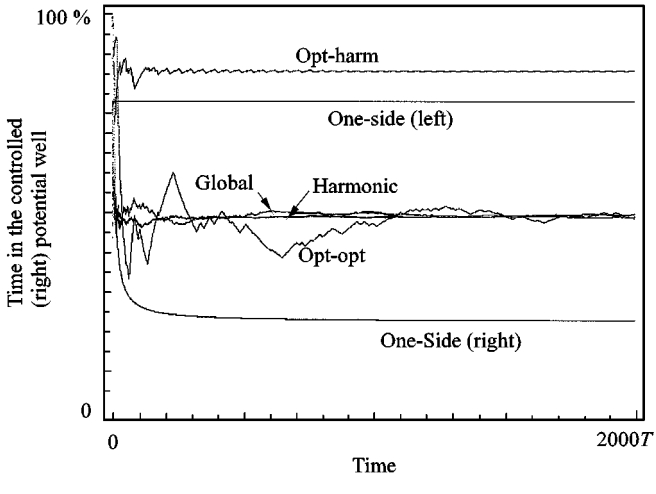

Figure 3. The percentage of time spent in the controlled (right) potential well for $\omega = 5$, $\gamma_1 = 3{\cdot}05$, $x_i = 0{\cdot}80$ and $\dot{x}_i = 0{\cdot}00$.

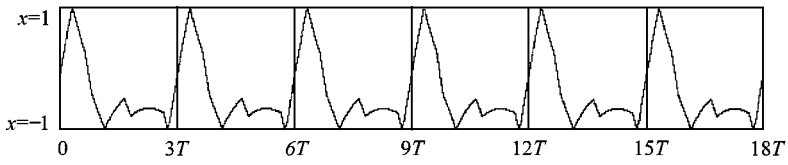

Figure 4. The time history of the period 3 scattered attractor, $\gamma_1 = 3{\cdot}05$.

case of one-side open-loop excitations, though this is in the non-controlled region. This example further shows that, according to the theoretical predictions, in the case of harmonic and global excitations, the mass spends one-half of the total time in each potential well. In the case of Figure 3 this holds also for the optimal–optimal implementation, although this is not be considered as a general property since this excitation is *not* actually symmetric due to its feedback nature.

It should be noted that, apart from the case of optimal–optimal excitation (which is of minor interest in this section), the asymptotical values are attained after 1000–1500 periods, ·which may be considered as the end of the transient dynamics.

An apparently unexpected phenomenon is that, for this value of γ_1, the right control permits the mass to be confined in the opposite (left) potential well. This is due to the fact that for this value of γ_1 the unique attractor is the period 3 scattered cycle shown in Figure 4 (compare with Figure 11 of reference [2, Part II]), which clearly spends the major part of the time in the left potential well. This circumstance is not completely surprising, because the region where the right control is effective in confining the dynamics in the right potential well extends up to $\gamma_1 = 2{\cdot}54$ (see reference [2, Part II]), a value which is well below $\gamma_1 = 3{\cdot}05$. By symmetry, obviously, the left control allows the mass to remain in the right potential well, and it is just this excitation that should be used if feedback control is not used.

4.2. SYSTEM GLOBAL ANALYSIS

4.2.1. *Behaviour charts in excitation parameter space*

In order to investigate how the time spent in the controlled well is influenced by the excitation parameters, Figure 5 shows two behaviour charts representing the percentage of time. In the parameter space (ω, γ_1), the square $4 \leqslant \omega \leqslant 6, 2 \leqslant \gamma_1 \leqslant 4$ is considered. It has been subdivided into 10×10 boxes and numerical simulations have been repeated for values of the parameters in the relevant vertices, always with i.c. $x_i = 0{\cdot}80$, $\dot{x}_i = 0{\cdot}00$, from $t = 0$ to $10000T$. The computations have been done with optimal–harmonic (Figure 5(a)) and with optimal–optimal (Figure 5(b)) excitations and at the end of each case we have reported the percentage of time spent in the controlled potential well. A smoothing algorithm has finally been employed.

Figure 5(a) guarantees that, according to the theoretical predictions, the optimal–harmonic excitation is very effective in the saved region (below the (thin) actual critical curve), being the percentage constantly greater than 70%. Furthermore, it is also effective above the actual critical curve and, in some cases, even beyond the (thick) theoretical critical curve. However, after a given threshold (which to a first approximation can roughly be said to correspond to $\gamma^r_{1,cr}$ on the basis of Figure 5(a) and of the assumed time represented scale), the performances reduce sharply and the implementation becomes ineffective.

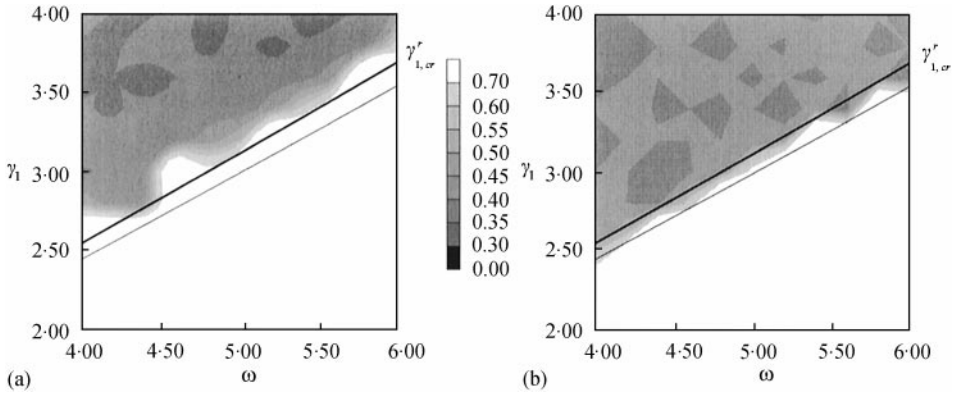

Figure 5. The percentage of the total time spent in the controlled (right) potential well. The thick line is the *theoretical* critical curve $\gamma^r_{1,cr}$, while the thin line is the corresponding *actual* threshold. These pictures correspond to $x_i = 0{\cdot}80$, $\dot{x}_i = 0{\cdot}00$ and $t = 10\,000T$. (a) Optimal–harmonic, (b) optimal–optimal.

Figure 5(b), on the other hand, shows that the other feedback implementation investigated is also effective in the actual saved region. However, contrary to the optimal–harmonic, the optimal–optimal excitation becomes ineffective just after the actual critical curve and it has no resources above the theoretical $\gamma^r_{1,cr}$. In this region, where scattered dynamics are largely predominant, its performances are comparable to those of the harmonic excitation (on average, one-half of the total time spent in each potential well) because, due to the numerous jumps between the two wells, the implementation becomes symmetric "on average", even if it is not geometrically symmetric.

Globally, Figure 5 confirms that the characteristics of the system response discussed in Figure 3 hold also for different values of the excitation parameters. In particular, it shows how the optimal–harmonic excitation allows the (white) region of good performances to enlarge toward large values of γ_1.

In the high excitation amplitude zone, localized zones of good performance (up to 100% of time in the time in the controlled well) may also exist. Indeed, it has been numerically obtained by Lenci and Rega in [2], and theoretically confirmed in [16] that, in the case of one-side control, stable bounded attractors can also exist above the theoretical critical curve: for example, a bounded inverse period doubling cascade based on a period 4 stable cycle exists for $\omega = 5$ and $\gamma_1 \in [2{\cdot}097, 3{\cdot}158]$ [2, Part II]. Being a bounded solution, the feedback implementation is never switched on and the mass spends all of the time in the controlled potential well, if the i.c. belong to the basin of attraction of the solution considered.

To illustrate this fact, Figure 6 shows a detailed section of the behaviour charts for $\omega = 5$, where the presence of a bounded solution is clearly recognizable: the overall curves are interrupted by the small window of 100% of time spent in the right well. The high-performance window, which is likely to be connected only to the large periodic window interrupting the region of cross-well dynamics in the bifurcation diagram of the one-side control (see Figure 9 in reference [2, Part II]), is not shown in Figure 5, where only the overall averaged behaviours are reported. In fact, though the occurrence of these periodic solutions certainly increases the performance of the control method, they are actually unrelated to the feedback implementations, being an intrinsic characteristic of the one-side (open-loop) optimal excitation. In any case, the comparison of the optimal–harmonic and optimal–optimal curves in Figure 6 confirms the overall advantage exhibited by the former

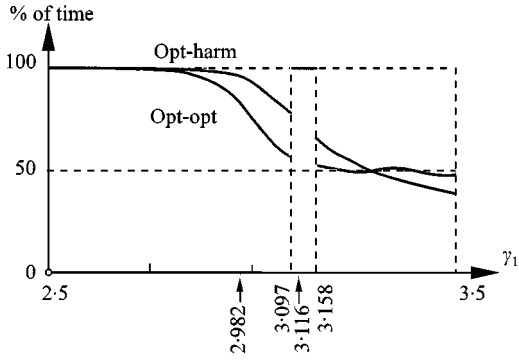

Figure 6. The percentage of the total time spent in the controlled (right) potential well for $\omega = 5$, $x_i = 0{\cdot}80$, $\dot{x}_i = 0{\cdot}00$ and $t = 10\,000T$. The *theoretical* critical threshold is $\gamma^r_{1,cr} = 3{\cdot}116$, while the corresponding *actual* one is 2·982.

excitation in the neighbourhood of the homoclinic bifurcation thresholds in terms of the performance parameter considered.

4.2.2. *Influence of the inial conditions*

The dependence of the system response with respect to i.c. is quite involved, and it is investigated in this section by extending the previous computations obtained for $x_i = 0{\cdot}80$, $\dot{x}_i = 0{\cdot}00$. Here, $\omega = 5$ and $\gamma_1 = 3{\cdot}05$ and variation of i.c are allowed. Initially, attention is focused on "long" transient dynamics, which deserves interest from a technical point of view.

The phase plane $-1 \leqslant x \leqslant 1, -2 \leqslant \dot{x} \leqslant 2$ has been subdivided into 50×50 boxes and, for values of the i.c. in the relative vertices, numerical simulations from $t = 0$ to $1000T$ have been performed for optimal–harmonic and for optimal–optimal excitations. The results are depicted in Figure 7 and 8 respectively.

The figures show that in both cases there is strong sensitivity with respect to i.c., and small variations may lead to different values of percentage of time spent in the controlled well. This fact may be justified by observing that, being in a region of high excitation amplitudes, these is an intrinsically chaotic region. Furthermore, after 1000 periods the steady regimes are not yet completely attained, as shown by Figure 9, and the sensitivity due to likely fractal basin boundaries becomes more marked in such transient regimes.

However, apart from the overall qualitative behaviour, there are strong differences concerning the technical performances. Indeed, it is observed that in the case of optimal–harmonic excitation (Figure 7) the computed time percentages oscillate around a mean value of 79·7%. Furthermore, on a large scale they depend little on i.c., and no point of Figure 7 is very far from the mean value (this is confirmed by the computed standard deviation which is equal to 0·046). These numbers confirm quantitatively the theoretically expected good performance of the optimal–harmonic implementation. On the contrary, the poor performance of the optimal–optimal implementation (which is actually of minor interest in this section and is reported only for comparison) are also confirmed quantitatively by the fact that the mean value is 42·1% and even on a large scale the oscillations around this value are not so small (compare the vertical scale in Figure 8 with that to Figure 7), as confirmed by the standard deviation which is equal to 0·167.

Increasing the excitation amplitude, the qualitative behaviour, and in particular the high dependence on a small scale and the low dependence on a large scale, is maintained, and the only differences are quantitative. For example, for $\omega = 5$ and $\gamma_1 = 3{\cdot}16$, in the case of

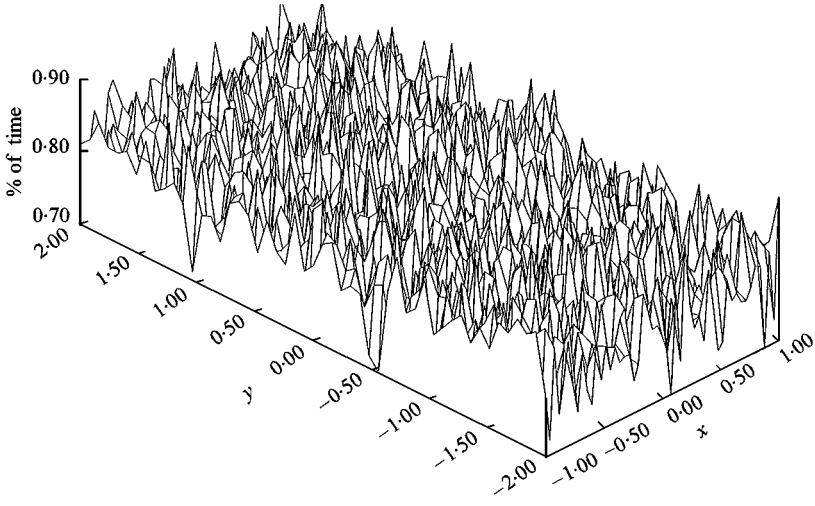

Figure 7. The time spent in the controlled (right) potential well in the case of optimal–harmonic excitation with varying i.c. ($y = \dot{x}$), $\omega = 5, \gamma_1 = 3{\cdot}05$ and $t = 1000T$.

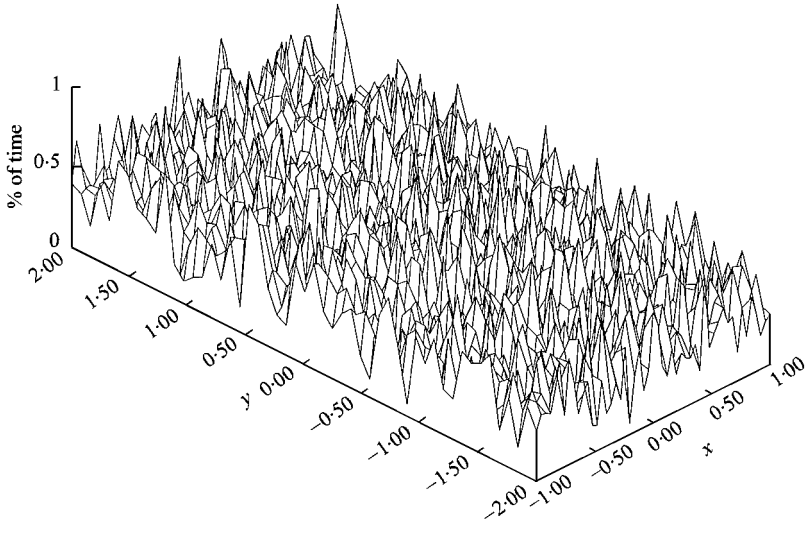

Figure 8. The time spent in the controlled (right) potential well in the case of optimal–optimal excitation with varying i.c. ($y = \dot{x}$), $\omega = 5, \gamma_1 = 3{\cdot}05$ and $t = 1000T$.

optimal–harmonic excitation, the mean time spent in the controlled potential well is 62·0% with standard deviation 0·033, while in the optimal–optimal case the mean value is 52·1% with standard deviation 0.060 (but still with large percentage peaks).

The good technical performance of the optimal–optimal excitation are also observed when prolonging the numerical simulations, as shown by Figure 9, where the time spent in the controlled well is reported for three different i.c. $(x_i, \dot{x}_i) = (0{\cdot}8, 0{\cdot}0)$, $(x_i, \dot{x}_i) = (0{\cdot}0,\ 0{\cdot}0)$ and $(x_i, \dot{x}_i) = (-0{\cdot}8, 0{\cdot}0)$. The variations tend to vanish and the asymptotic 85% (larger than the previously determined mean value) is approached, so that the effectiveness is maintained in time. On the other hand, the unsatisfactory performances

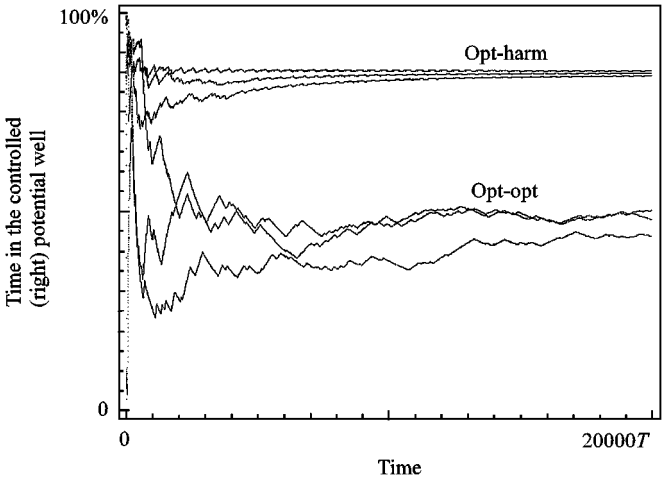

Figure 9. The time spent in the controlled (right) well for i.c. $(x_i, \dot{x}_i) = (0{\cdot}8, 0{\cdot}0), (x_i, \dot{x}_i) = (0{\cdot}0, 0{\cdot}0)$ and $(x_i, \dot{x}_i) = (-0{\cdot}8, 0{\cdot}0)$, $\omega = 5$ and $\gamma_1 = 3{\cdot}05$.

of optimal–optimal implementation are also confirmed, because the variations do not tend to vanish, even if they diminish. A mean value slightly lesser that 50% is approached.

5. THE REDUCTION OF JUMPS

Both the implementations discussed, and in particular the optimal–optimal one, are aimed at reducing the number of jumps from one to the other potential well.

To make this statement more precise, a rigorous definition of a jump is given; it is the time interval between the first impact on the right (left) rigid constraint and the first subsequent impact on left (right) restraint. This definition is depicted in Figure 10. Note that, in this way, the time history can be viewed as a sequence of jumps if the solution switches between the two potential wells, or as a unique jump if the solution always remains in the same part of the phase space. It is worth emphasizing that, by definition, the proposed implementations will give satisfactory results if they allow the number of jumps with respect to the open-loop excitations to be reduced.

5.1. SYSTEM LOCAL ANALYSIS

For the case of Figure 3, and referring to the same numerical tools, parameters and reference i.c. as employed in the previous sections, the number of jumps is plotted versus time in Figure 11. An inial temporal window $0 \leqslant t \leqslant 1000T$ is illustrated, showing that the feedback implementations greatly reduce the number of jumps: in the case of Figure 11, with the optimal–harmonic excitation it is reduced, more or less, to 1/5, while with the optimal–optimal excitation the number of jumps is, say, 1/10 of the best open-loop excitation, which in this case is the global one. As expected, the optimal–optimal implementation gives the best result and it is very effective.

In Figure 11, the curve for the number of jumps in the case of one-side control is a straight line. In fact, as shown in Figure 4, in this case the periodic solution performs two jumps for every 3 periods of the external excitation. Thus, apart from the short initial transient, the

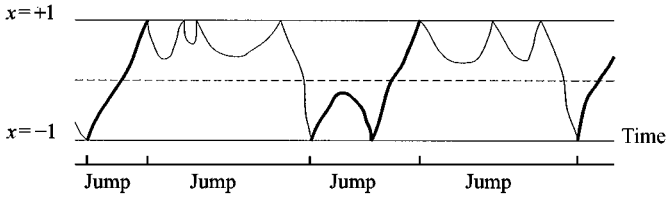

Figure 10. The definition of jumps.

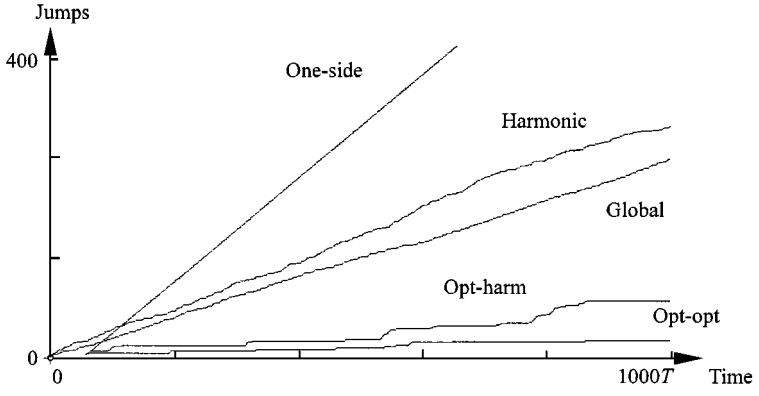

Figure 11. The number of jumps versus time for $\omega = 5, \gamma_1 = 3{\cdot}05, x_i = 0{\cdot}80$ and $\dot{x}_i = 0{\cdot}00$.

number of jumps is exactly linear with slope 0·667. Also the other curves shown in Figure 11 seem to be approximated by linear functions, and it is important to check whether this property is maintained in the steady regime. To this purpose, the relevant numerical integrations were continued up to $t = 20\,000T$ and Figure 12 shows the slopes of the least-squares homogeneous linear approximations of the number of jumps. They tend to the well-defined asymptotic values 0·022, 0·057, 0·263, 0·292 and 0·667, from bottom to top. Figure 12 also shows that the asymptotic values are attained in $1000–2000T$. This is an *a posteriori* check that Figure 11 actually describes the transient as well as the steady state behaviour of the system.

In the following sections, the influence of the feedback implementations on the performance of the system with respect to the case of open-loop excitations are analyzed in more detail. To measure quantitatively the improvements, the harmonic excitation is considered as reference. This choice is justified by the fact that, as shown in Figure 12, global and harmonic excitations give more or less the same performances in terms of reduction of the number of jumps, while the one-side control gives the worst results. So, any improvement with respect to the harmonic excitation is an improvement with respect to the global control and, *a fortiori*, an improvement with respect to the one-side control.

5.2. SYSTEM GLOBAL ANALYSIS

5.2.1. *Behaviour charts in excitation parameter space*

In order to check the overall effectiveness of the implementations, a direct comparison between the number of jumps obtained with the proposed excitations and that with the reference (harmonic) excitation, should be made for different values of the parameters.

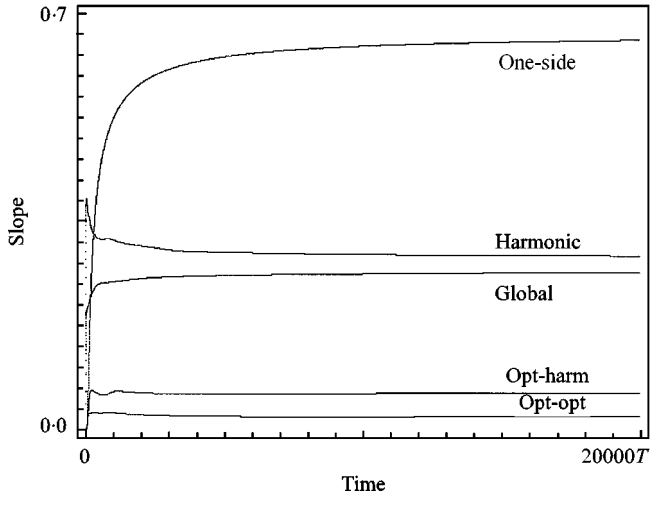

Figure 12. The slopes of the best lines approximating the curves of Figure 11.

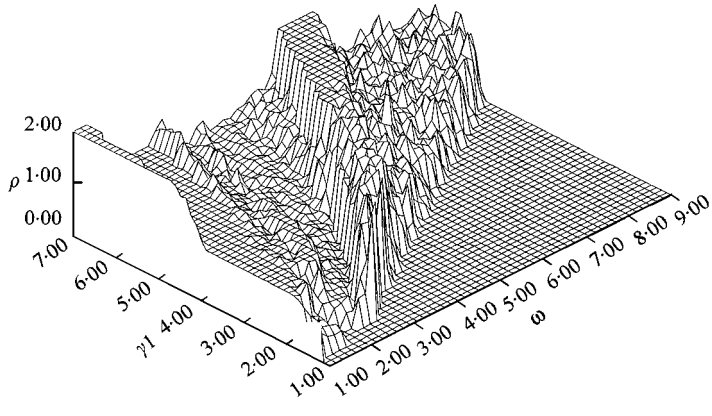

Figure 13. The coefficient ρ in the case of optimal–harmonic excitation for different values of the parameters and for $x_i = 0{\cdot}80$, $\dot{x}_i = 0{\cdot}00$ and $t = 1000T$.

To synthesize and to obtain a quantitative measure of the properties of the implementations, a *coefficient of reduction of jumps* ρ is introduced, which is defined as the ratio between the number of jumps corresponding to the implementation considered and the one corresponding to the harmonic (reference) excitation. By definition, the implementation works well if it gives values of ρ lesser than one, while it should be disregarded in the opposite case.

When there are no jumps with harmonic excitation, ρ is not defined. The convention of setting $\rho = 0$ is adopted in these cases. Here, of course, the implementations are not required because the harmonic excitation gives already satisfactory results.

In the parameter space (ω, γ_1), the region $1 \leqslant \omega \leqslant 9$, $1 \leqslant \gamma_1 \leqslant 7$ will be analyzed. This rectangle is subdivided in 50×50 boxes and numerical simulations are performed for values of the parameters in the approximate vertices, always with i.c. $x_i = 0{\cdot}80$, $\dot{x} = 0{\cdot}00$ from $t = 0$ to $1000T$. The computations have been done with harmonic, optimal–harmonic and optimal–optimal excitations, and at the end of each step the two reduction coefficients have been calculated. The results are reported in Figures 13 (optimal–harmonic) and 14

(optimal–optimal). To draw these figures, a cut-off at $\rho = 2$ has been introduced for graphical reasons.

In both cases, ρ is not a flat function of ω and γ_1: apart from the zones where it is approximately equal to zero, it varies on a small scale, showing some sort of sensitivity with respect to the parameters.

The main feature of Figure 14 is that there is a well-defined zone where ρ is greater than 1, which consists of small neighbourhoods of the cut-off regions in the Figure. In the remaining part of the diagram, ρ is considerably lesser than the unity, showing the effectiveness of the optimal–optimal implementation in reducing the number of jumps. Furthermore, the transition from one to the other zone in quite sharp. Figure 13 shows a different pattern of behaviour. Here the cut-off zone is smaller, but in the remaining parts the coefficient of reduction is not very different from 1, both when $\rho > 1$ and when $\rho < 1$.

A comparison between the two cases shows that, as expected, the optimal–optimal implementation is much more effective in reducing the number of jumps than the optimal–harmonic.

Basically, the plane (ω, γ_1) can be subdivided into three parts: one where the implementations allow the number of jumps to reduce $(0 < \rho < 1)$; one where they should be disregarded $(\rho \geqslant 1)$ and, finally, the one where the harmonic excitation gives zero jumps. These regions are reported in grey, black and white, respectively, in Figures 15 and 16. It is worth comparing the performance in terms of jump reduction with the saved chaotic region. Accordingly, the critical curve for the harmonic excitation, the actual critical curve for the two-impulse approximation of the optimal $f(t)$ and the theoretical critical curve for $c = -5$ (see Figure 2), are also given in the two figures from bottom upwards.

Qualitatively, Figures 15 and 16 are similar to each other, even if in the grey regions the optimal–optimal implementation gives better results, as previously emphasized. In both cases, the grey region extends above the approximate critical curve and also above the theoretical one $\gamma^r_{1,cr}$, while the black regions (where there are highly cross-well chaotic dynamics) have a typical shape of two "narrow" cones, one vertical and the other oblique.

There are two remarkable characteristics in Figures 15 and 16. The first is that the boundaries between the grey and white regions correspond, in the first approximation, to

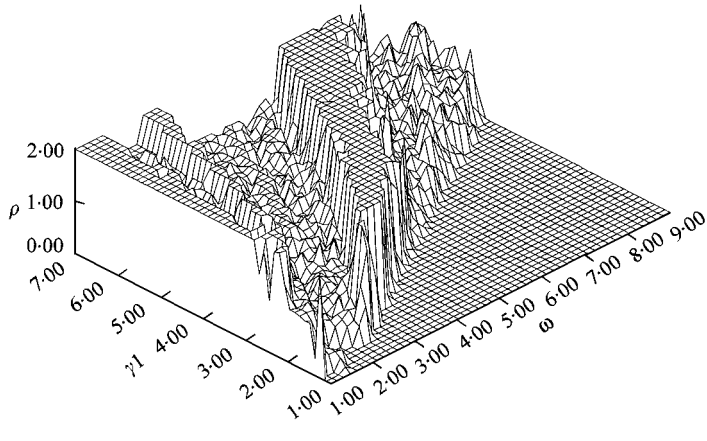

Figure 14. The coefficient ρ in the case of optimal–optimal excitation for different values of the parameters and for $x_i = 0{\cdot}80$, $\dot{x}_i = 0{\cdot}00$ and $t = 1000T$.

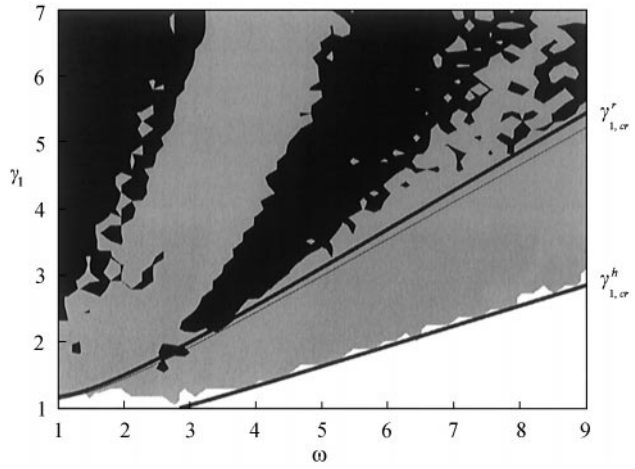

Figure 15. Behaviour chart with optimal–harmonic implementation for $x_i = 0{\cdot}80$, $\dot{x}_i = 0{\cdot}00$ and $t = 1000T$. (grey, $0 < \rho < 1$; black, $\rho \geqslant 1$; white, $\rho = 0$).

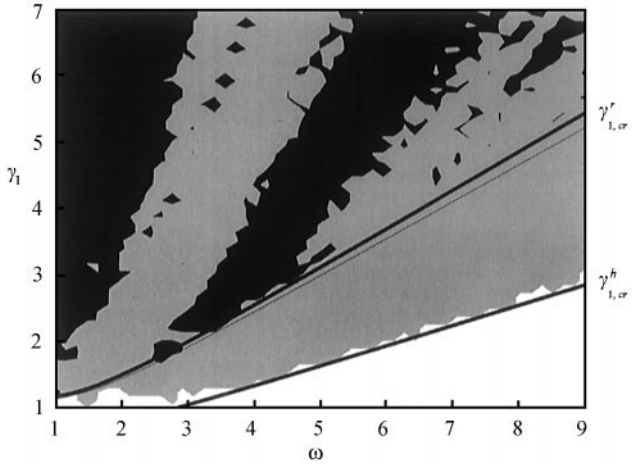

Figure 16. Behaviour chart with optimal–optimal implementation for $x_i = 0{\cdot}80$, $\dot{x}_i = 0{\cdot}00$ and $t = 1000T$. (grey, $0 < \rho < 1$; black, $\rho \geqslant 1$; white, $\rho = 0$).

the curve $\gamma^h_{1,cr}$; this confirms, and generalizes to the overall excitation parameter space, that the cross-well spread of the solution is greatly influenced by the transverse homoclinic intersection, as already shown in reference [2] for isolated frequency values. Indeed, $\gamma^h_{1,cr}$ is not only the theoretical critical curve for fractal basin boundaries and associated transient chaotic dynamics, but also the practical threshold for the scattered character of the oscillations of the system subjected to the harmonic excitation.

The second unexpected circumstance that must be highlighted is the occurrence in both cases of an obliquely striped grey region above the lower black one. Thought the implementations are not very effective in these zones where ρ is, on average, greater than 0·9, this is particularly surprising, because it was natural to conjecture the existence of a unique critical value, say $\gamma^{imp}_{1,cr}(\omega)$, such that $\rho > 1$ for all $\gamma_1 > \gamma^{imp}_{1,cr}$. This fact shows unforeseen properties of the proposed implementations, at least for the chosen i.c.

5.2.2. *Influence of the initial conditions*

The above numerical integrations have been performed with the fixed i.c. $x_i = 0{\cdot}80$, $\dot{x}_i = 0{\cdot}00$. In order to perform a sensitivity analysis the variation of the coefficient ρ with different i.c. is now analyzed for fixed values of the excitation parameters $\omega = 5$ and $\gamma_1 = 3{\cdot}16$. In the parameter plane, this point is just above the theoretical critical threshold $\gamma'_{1,cr}(\omega = 5) = 3{\cdot}116$, i.e., in the grey region. As in section 4.2.2, the phase plane $-1 \leqslant x \leqslant 1, -2 \leqslant \dot{x} \leqslant 2$ is subdivide into 50×50 boxes and numerical simulations from $t = 0$ to $1000T$ performed. The computations have been done with harmonic, with optimal–harmonic and with optimal–optimal excitations and at the end of each step the two reduction coefficients have been calculated. The results are reported in Figures 17 (optimal–harmonic) and 18 (optimal–optimal).

Figures 17 and 18 emphasize three main characteristics, which seem to confirm the dependence of ρ on the i.c. in the "long" transient dynamics, and which partially resemble those observed in section 4.2.2.

(i) On a small scale, there is strong dependence on i.c. Slight variations of i.c. lead to different values of ρ. There appears to be some kind of sensitivity of the response, possibly because, in parameter space, there is an intrinsically cross-well chaotic point under harmonic excitation.
(ii) On a large scale, on the other hand, there is little dependence on i.c. Indeed, every value of ρ reported in Figures 17 and 18 is not very far from the corresponding mean values, which are $\rho = 0{\cdot}585$ and $\rho = 0{\cdot}282$ respectively. This shows the almost uniform behaviour of the two implementations and further confirms that the optimal–optimal implementation gives the best results, in terms of reduction of jumps.
(iii) The two implementations behave qualitatively in the same manner, and the only differences are of quantitative nature.

Running the numerical simulations for longer leads to partially smoothing out the variations of ρ with respect to i.c., as shown in Figure 19, which is drawn for the same ω and γ_1 as Figures 17 and 18. In this figure, the coefficient of reduction of jumps is reported for

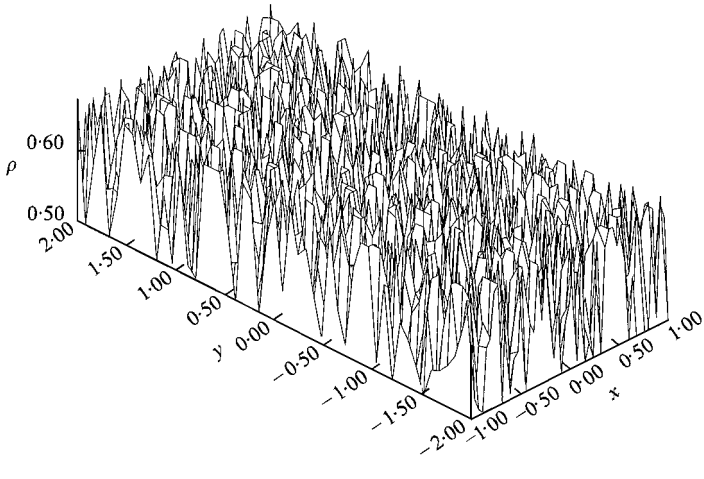

Figure 17. The coefficient ρ in the case of optimal–harmonic excitation with varying i.c. ($y = \dot{x}$). $\omega = 5$, $\gamma_1 = 3{\cdot}16$ and $t = 1000T$.

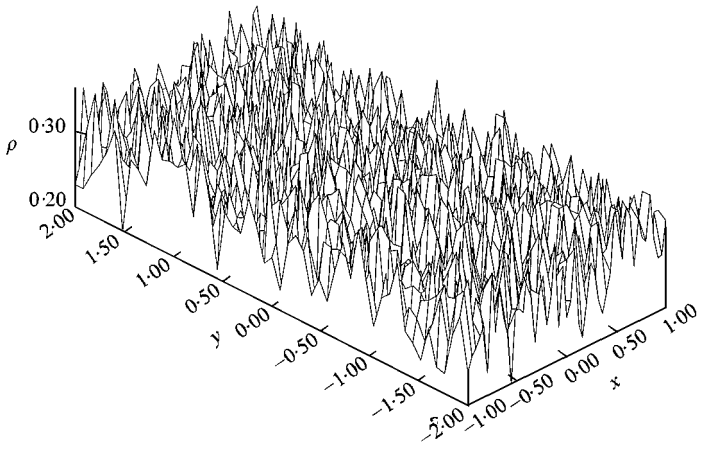

Figure 18. The coefficient ρ in the case of optimal–optimal excitation with varying i.c. ($y = \dot{x}$). $\omega = 5$, $\gamma_1 = 3{\cdot}16$ and $t = 1000T$.

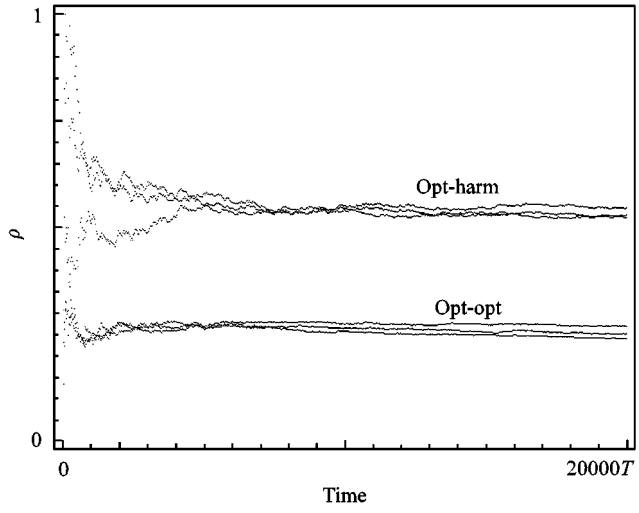

Figure 19. The coefficient of reduction of jumps for i.c. $(x_i, \dot{x}_i) = (0{\cdot}8, 0{\cdot}0)$, $(x_i, \dot{x}_i) = (0{\cdot}0, 0{\cdot}0)$ and $(x_i, \dot{x}_i) = (-0{\cdot}8, 0{\cdot}0)$, $\omega = 5$ and $\gamma_1 = 3{\cdot}16$.

three different i.c. $(x_i, \dot{x}_i) = (0{\cdot}80, 0{\cdot}0)$, $(x_i, \dot{x}_i) = (0{\cdot}0, 0{\cdot}0)$ and $(x_i, \dot{x}_i) = (-0{\cdot}8, 0{\cdot}0)$. It is seen that, after the initial transient, the variations of ρ tend to vanish. It is worth noting that ρ remains constantly below 1, this property showing that the effectiveness of the method is maintained in time. Furthermore, note that the asymptotic values are close to the mean values reported in previous point (ii).

Further understanding of the influence of the i.c. would require identifying and characterizing the (possibly competing) chaotic and periodic attractors, and their basins of attraction and in analyzing the modifications induced by system parameters variations, which is a dynamical system point of view. Herein, the interest is mostly on some performances of the feedback procedure (i.e., the average $\rho < 1$ value) and, from this standpoint, there is low dependence on i.c.

6. THE EFFECTS OF THE IMPLEMENTATIONS ON THE ACTUAL DYNAMICS

This section is aimed at highlighting how the proposed implementations achieve, in terms of actual dynamics, the technical performance discussed in the previous sections. As a by-product, this permits the comparison of the actual dynamics of the feedback with the open-loop excitations. The response in the temporal windows $0 \leqslant t \leqslant 1000T$ starting from $x_i = 0{\cdot}80$ and $\dot{x}_i = 0{\cdot}00$ will be shown, which, at least in the illustrative examples, are sufficient to capture the qualitative *steady* state character of the solutions and posses all the main features it is wished to highlight.

Figure 20 reports the time histories when the system is subjected to optimal–harmonic (Figure 20(a)) and optimal–optimal (Figure 20(b)) excitations. It shows the main features of the feedback implementations described in section 3.1 and 3.2. When the solution remains in the right potential well (upper part of each row in the Figure), the right control governs the system response producing bounded oscillations on the right barrier. When the orbit escapes, according to the theoretical predictions the optimal–harmonic implementation gives rise to chaotic dynamics which drive again the solution to the upper part. The time of right well targeting may be very short or somewhat longer, but bounded oscillations on the right are always recovered. The motion consists of a sequence of largely prevalent, bounded, fairly regular, oscillations on the right interrupted by short-duration cross-well chaotic oscillations.

With the optimal–optimal implementations, on the other hand, when the mass escapes form a potential well, it performs bounded oscillations in the other part of the phase space as long as it falls again in the previous well, and so on. These mechanisms of control correspond strictly to the theoretical predictions. Thus, the motion consists of a sequence of bounded, fairly regular oscillations on the right and on the left part of the phase space, which, on average, are equally extended. It should be noted how the time required to switch from one to the other bounded oscillation is very short (at least in the case reported in Figure 20(b)).

For the same values of the parameters, the steady dynamics of the system subjected to one-side control is the cross-well period 3 attractor shown in Figure 4, while those corresponding to harmonic and global optimal excitations are depicted in Figure 21. These latter are completely irregular, fully scattered and chaotic. Thus, the feedback implementations also permit a regularization of the system dynamics with respect to the harmonic and global excitation, though the best regularization is furnished by the one-side optimal control. However, the latter is likely to be a non-generic and non-requested feature of the related controlled dynamics.

7. CONCLUSIONS

Two shrewd implementations of an optimal procedure for controlling non-linear transient and steady dynamics of mechanical systems previously developed by the authors have been discussed. They are aimed at improving some technical performances of two-well potential systems related to the necessity of reducing the scattered character of the dynamics for high amplitude values of the external excitation, where open-loop controls are in general much less efficient.

The proposed strategies, which consist of applying an alternation of first, right optimal and harmonic excitations, and of second, right and left optimal excitations, meet some specific practical requirements, two of which have been analyzed in detail. The former is the possibility of increasing the time spent by the hitting mass in one of the two potential wells, while the latter is the reduction of the number of potentially dangerous jumps between the

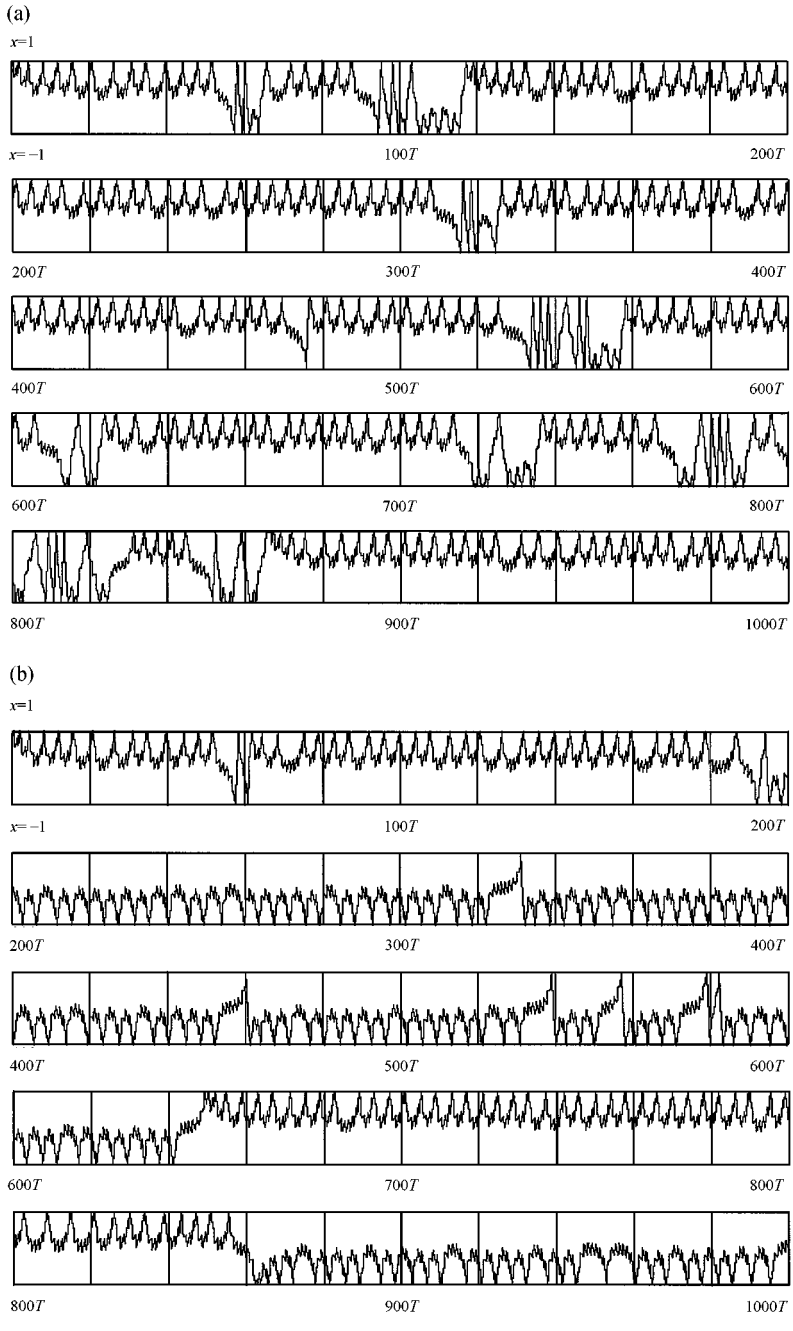

Figure 20. Time histories for $\omega = 5$ and $\gamma_1 = 3{\cdot}05$; feedback excitations. (a) Optimal–harmonic excitation, (b) optimal–optimal excitation.

two wells. A parameter of reduction of jumps have been introduced to synthesize and quantify the effectiveness of the proposed implementations.

It has been shown how the optimal–harmonic excitation permits an increase in the percentage of time spent by the mass in the desired potential well. This fact, has been illustrated both for specific values of the excitation parameters, and with reference to

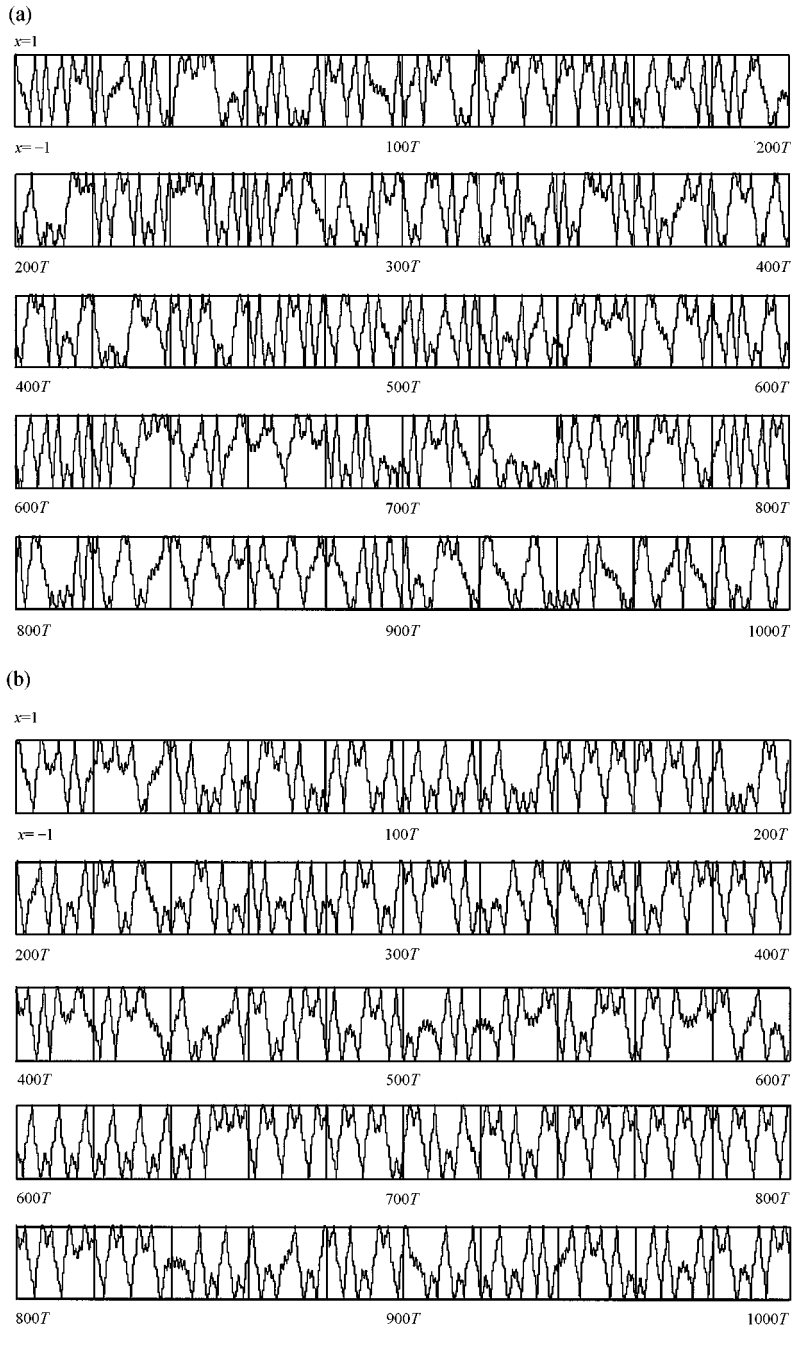

Figure 21. Time histories for $\omega = 5$ and $\gamma_1 = 3{\cdot}05$; open-loop excitations. (a) Harmonic excitation, (b) global excitation.

behaviour charts obtained in the overall parameter space. They show how the optimal–harmonic excitation permits an enlargement of the region of effectiveness in terms of confinement towards high values of γ_1, even well above the theoretical critical curve for chaos. The robustness of such a performance with respect to variations of initial conditions has also been illustrated.

Coherently with the theoretical predictions, it has been shown through systematic numerical simulations that the two implementations, and mostly the optimal–optimal excitation, permit a considerable reduction in the number of jumps. Again, this has been checked both locally, showing how the number of jumps depends on time in some cases, and globally, by means of contour plots of the jump reduction coefficient ρ as a function of the frequency and magnitude of the excitation. The dependence of ρ on the initial conditions has been investigated in both transient and steady dynamics, showing that it tends to vanish in the latter case. In any case, from the standpoint of performances of the feedback (i.e., obtaining an average $\rho \leqslant 1$ value), there is fairly low dependence on inial conditions.

The mechanisms through which the implementations permit the control of the dynamics have been analyzed by means of some time histories, comparing and discussing the performance of the feedback and of the open-loop excitations.

It is also worth noting that the feedback control strategies adopted here are based on only rough information about the state of the system, and this can be viewed as a type of robustness in a general sense.

For a complete description of the system global dynamics, a systematic bifurcation analysis aimed at analyzing and computing the effects of alternative control procedures [2], would be needed. However, from the viewpoint of this paper, it has been worth highlighting how a procedure formulated within the dynamical system theory for optimally controlling (transient) chaos, shows itself also capable, if properly implemented, of fulfilling important technical requirements of the system steady response.

The proposed implementations allow an improvement in the system performance not only in the highest part of the save regions, but also beyond, and sometimes much above (see Figures 15 and 16), the theoretical critical threshold for chaos, thus showing partially unforeseen resources of the feedback. Though in these regions it cannot be expected that the whole system dynamics are regularized (as it should occur, on average, in the saved regions), the improvement of the technical performances can again be considered to be a satisfactory result of the proposed method.

In this respect, the feedback is the suitable modification of the open-loop control aimed at improving its performances for high values of the amplitude. Thus, in some vague sense, one could say that no control is required for low γ_1's, open-loop control must be used for medium values of γ_1 and feedback control is necessary for high γ_1's. In this hypothetical scale, the general performances of the control are substantially preserved, passing for the "natural" confinement and regularization of the system non-linear dynamics obtained with the open-loop optimal excitations [2] to the effective technical performances realized through the numerical feedback control illustrated in this paper.

At least two developments of the present analysis can be pursued. One refers to the possibility of physical experimentations, while the other is concerned with application of procedures for reducing scattering to different, and more general, systems. In a number of cases, this can be done analytically in conjunction with the classical Melnikov's method [18].

ACKNOWLEDGMENT

The financial support of Italian M.U.R.S.T. is acknowledged. The authors thank one reviewer for useful comments.

REFERENCE

1. S. LENCI and G. REGA 1998 *Nonlinear Dynamics* **15**, 391–409. A procedure for reducing the chaotic response region in an impact mechanical system.

2. S. LENCI and G. REGA 1998 *International Journal of Bifurcation and Chaos* **8**, 2387–2424. Controlling nonlinear dynamics in a two-well impact system. Parts I and II.
3. S.W. SHAW 1990 *Nonlinear Dynamic in Engineering Systems*, (W. Schiehlen editor). Proceedings of IUTAM Symposium, Stuttgart Germany August 21–25, 1989. Berlin: Springer-Verlag. The suppression of chaos in periodically forced oscillators.
4. A. ISIDORI 1995 *Nonlinear Control Systems*. Rome: Springer-Verlag.
5. F. L. CHERNOUSKO 1996 *Proceedings of 2nd European Nonlinear Oscillations Conference*, Vol. 1, 15–22 Prague, September 1996. Control of nonlinear dynamical systems.
6. B. BLAZEJCZYK, T. KAPITANIAK, J. WOJEWODA and J. BRINDLEY 1993 *Applied Mechanics Review* **46**, 385–391. Controlling chaos in mechanical systems.
7. T. KAPITANIAK 1996 *Controlling Chaos*. Lodz: Academic Press.
8. E. OTT, C. GREBOGI and J. A. YORKE 1990 *Physical Review Letters E* **64**, 1196–1199. Controlling chaos.
9. G. CHEN and X. DONG 1993 *International Journal of Bifurcation and Chaos* **3**, 1363–1409. From chaos to order—perspectives and methodologies in controlling chaotic nonlinear dynamical systems.
10. R. LIMA and M. PETTINI 1990 *Physical Review A* **41**, 726–733. Suppression of chaos by resonant parametric perturbations.
11. G. CHEN and X. DONG 1998 *From Chaos to Order*: *Methodologies Perspectives and Applications*. Singapore: World Scientific Publications.
12. B. BROGLIATO 1999 *Nonsmooth Mechanics*. London: Springer-Verlag.
13. S. LENCI and G. REGA 1996 *Nonlinear Dynamics and Control* (A. K. Bajaj, N. S. Namachchivaya and M. A. Franchek editors). *Proceedings of ASME International Mechanical Engineering Congress*, Vol. **DE-91**, 111–116. Global chaos control in a periodically forced oscillator.
14. S. LENCI and G. REGA 1997 *Control of Oscillations and Chaos*, (F. L. Chernousko and A. L. Fradkov, editors) *Proceedings of the* 1*st International Conference COC*'97 Vol. **3**, 582–585. Attractor-basin and bifurcation analysis in an impact system: chaotic uncontrolled versus controlled steady response.
15. S. LENCI and G. REGA 1997 *Proceedings of* 1997 *ASME Design Engineering Technical Conference*, *Sacramento*, *CA*, *U.S.A.*, 14–17 September DETC97/VIB-4014. Feedback numerical implementations of an optimal procedure for chaos control in a two-well impact oscillator.
16. S. LENCI and G. REGA 1998 *Dynamics of Vibro-Impact System* (V. I. Babitsky, editor) *Proceedings of Euromech Colloquium* 15–18 *September*, 167–176. Interaction between impulses and impacts in the nonlinear dynamics of an impacting system: a non-classical bifurcation.
17. S. LENCI 1998 *SIAM Journal on Applied Mathematics* **58**, 1116–1127. On the suppression of chaos by means of bounded excitations in an inverted pendulum.
18. S. WIGGINS 1990 *Introduction to Applied Nonlinear Dynamical Systems and Chaos*. New York: Springer-Verlag.